Final Technical Report - DE-SC0008998

A Novel Multi-scale Simulation Strategy for Turbulent Reacting Flows

2012-2017

James C. Sutherland, Associate Professor, The University of Utah

Abstract

In this project, a new methodology was proposed to bridge the gap between Direct Numerical Simulation (DNS) and Large Eddy Simulation (LES). This novel methodology, titled Lattice-Based Multiscale Simulation (LBMS), creates a lattice structure of One-Dimensional Turbulence (ODT) models. This model has been shown to capture turbulent combustion with high fidelity by fully resolving interactions between turbulence and diffusion [1, 2]. By creating a lattice of ODT models, which are then coupled, LBMS overcomes the shortcomings of ODT, which are its inability to capture large scale three dimensional flow structures. However, by spacing these lattices significantly apart, LBMS can avoid the curse of dimensionality that creates untenable computational costs associated with DNS. This project has shown that LBMS is capable of reproducing statistics of isotropic turbulent flows while coarsening the spacing between lines significantly. It also investigates and resolves issues that arise when coupling ODT lines, such as flux reconstruction perpendicular to a given ODT line, preservation of conserved quantities when eddies cross a course cell volume and boundary condition application. Robust parallelization is also investigated.

1 Introduction

The ODT model is able to fully resolve length and time scales while still remaining computationally cost effective. By fully resolving these scales, ODT creates high fidelity simulations of buoyant flows, stratified flows and combusting flows [3, 4, 5]. However, as a one dimensional model, it fails to capture any large scale phenomena such as recirculation, complex geometry, *etc.*

LBMS is a novel methodology that accounts for the three dimensional nature of many complex flows while both resolving small scale turbulent interactions as well as remaining computationally tenable. This methodology is a lattice like structure of ODT models, as depicted in Figure 1. The fine spacing, δ, is the resolution required for the smallest spatial structures in the flow field. The coarse spacing, Δ, is the spacing between each individual line (on the order of the integral length scale), and all lines in a given direction form a *bundle*.

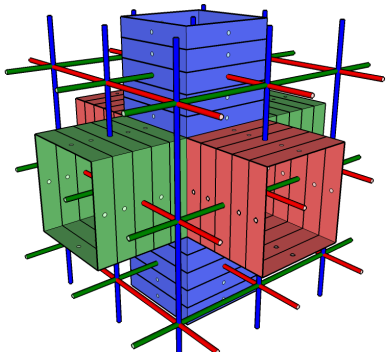

Figure 1: Representation of a 3D LBMS mesh. Each color denotes a different directional bundle. Lines are fully resolved.

1.1 Significance

There are a wide variety of difficult problems in turbulence that ODT can tackle with the high-fidelity coupling of diffusive and convective effects across the range of turbulent length scales. By building a lattice of these models, LBMS will utilize this to capture large scale, three dimensional effects. For a three-dimensional domain, with θ unknowns and a uniform grid spacing of δ in every dimension, a traditional DNS simulation has $\theta\left(\frac{L}{\delta}\right)^3$ unknowns to be solved for. LBMS, on the other hand, has three overlaying domains with grid spacings $\delta\Delta^2$ and thus has to solve for $3\theta\frac{L^3}{\delta\Delta^2}$ unknowns. Length scales in turbulent flows scale at $Re^{3/4}$ [6]. Therefore, the costs of a three-dimensional DNS simulation will scale at $Re^{9/4}$. Computational costs become exponentially prohibitive for a DNS study in very turbulent flows. If $\delta \ll \Delta$, then LBMS scales at roughly $Re^{3/4}$. With LBMS only needing to resolve the large scale features at the coarse level, $\delta \ll \Delta$ will almost always be true, particularly for highly turbulent flows. Table 1 shows how LBMS can bridge the gap between DNS and LES simulations by rendering computationally cost prohibitive problems in DNS tractable while resolving the smallest scale features and their couplings that traditional LES misses.

Table 1: Comparison of scaling requirements of DNS, LBMS and LES simulations based off of the Reynolds number associated with the flow.

	DNS	LBMS	LES
# of θ	$\theta\left(\frac{L}{\delta}\right)^3$	$3\theta\frac{L^3}{\delta\Delta_{LBMS}^2}$	$\theta\left(\frac{L}{\Delta_{LBMS}}\right)^3$
Re scaling requirements	$Re^{9/4}$	$Re^{3/4}$	$Re^{0.5} - Re^2$ [7]

1.2 Potential Applications

The power and utility of ODT lies in its ability to fully resolve all convective transport, diffusive transport and their coupling across all length scales associated with a highly turbulent flow without demanding unreasonable computational costs [2]. There are nearly an infinite number of problems for which this has proven useful. Shear flows, buoyant stratified flows and mixing layers are dependent on this interaction; ODT captures the underlying physics with high fidelity [2, 8, 9, 3]. Non-premixed combustion requires the diffusion of oxidizer and fuel to the flame front but the underlying chemistry imbues these problems with incredible stiffness. The ability to capture diffusive-convective interactions cheaply has propelled ODT through the combustion community, where turbulent mixing is often used to increase the rate of reactions in various applications [10, 11, 5]. The fidelity is sufficient to capture particularly difficult combustion problems, such as ignition, soot formation and extinction [4, 12]. ODT can even simulate particle-laden fluid flows, where small scale diffusion can be an important driving force in coal combustion or particle-particle agglomeration [13, 14].

2 Formulation

2.1 Governing Equations

Our generalized balance equations are written in finite-volume form as

$$\int_{\mathsf{V}(t)} \frac{\partial \rho\psi}{\partial t}\,\mathrm{d}\mathsf{V} = -\int_{\mathsf{S}(t)} \mathbf{\Theta}_\psi \cdot \mathbf{n}\,\mathrm{d}\mathsf{S} + \int_{\mathsf{V}(t)} \sigma_\psi\,\mathrm{d}\mathsf{V}, \tag{1}$$

where ψ is the transported variable, $\mathbf{\Theta}_\psi$ is the total flux of ψ and σ_ψ is the volumetric source term. LBMS uses an Eulerian formulation to alleviate complexities with bundle interactions. This formulation implies that the control volumes are temporally fixed. This is necessary to ensure that the bundles can communicate with each other. ψ and the associated terms are given by Table 2.

Table 2: Quantities in (1) for each governing equation. $\boldsymbol{u}$ represents the velocity, ρ the density, $\boldsymbol{\tau}$ is the stress tensor, p represents the pressure, $\boldsymbol{g}$ the gravitational acceleration, e_0 the total internal energy, $\boldsymbol{q}$ the energy diffusive flux, Y_i the mass fraction of species i, $\boldsymbol{j_i}$ the diffusive flux of species i and σ_i the reaction rate of species i.

Equation	ψ	Total Flux, $\mathbf{\Theta}_\psi$	Source Term, σ_ψ
Mass	1	$\rho\mathbf{u}$	0
Momentum	$\mathbf{v}$	$p\mathbf{I} + \boldsymbol{\tau} + \rho\mathbf{u}\mathbf{u}$	$\rho\mathbf{g}$
Species	Y_i	$\rho \mathrm{Y}_i\mathbf{u} + \mathbf{j}_i$	σ_i
Total Internal Energy	e_0	$e_0\mathbf{u} - p\mathbf{u} - \boldsymbol{\tau}\cdot\mathbf{u} + \mathbf{q}$	$\rho\mathbf{g}\cdot\mathbf{u}$

2.2 Triplet Mapping

The eddy events are applied to solution variables between temporal (or spatial) steps. In this sense, the rearrangement can be thought of as instantaneous. Each eddy event is executed through a triplet mapping function, shown in Equation 2, $f(x)$. This is represented graphically in Figure 2. In this case, x_0 represents the initial coordinate of the eddy and l represents its length.

$$f(x) = \begin{cases} x_0 + \frac{1}{3}(x - x_0) \\ x_0 + \frac{2}{3}l - \frac{1}{3}(x - x_0) \\ x_0 + \frac{2}{3}l + \frac{1}{3}(x - x_0). \end{cases} \tag{2}$$

As this mapping is a continuous function of $f(x)$, discontinuities are prevented from forming. This application as applied to a velocity field is represented as

$$u_i(x) \rightarrow u_i f((x)) + c_i K(x), \tag{3}$$

where c_i and K are kernel operators that ensure conservation of momentum in the presence of pressure gradients. As realized in turbulent flows, two neighboring fluid parcels will remain nearby. Furthermore, this rearrangement of information captures the rotational and compressive nature of turbulence, again shown in Figure 2 [2]. c_i is given by

$$c_i = \frac{27}{4l}\left(-\hat{u}_i + sign(\hat{u}_i)\sqrt{\frac{1}{2}\left(\hat{u}_i^2 + \hat{u}_j^2 + \hat{u}_k^2\right)}\right) \tag{4}$$

where $\hat{u}$ is

$$\hat{u_i} = \frac{1}{l^2}\int u_i(f(x))K(x)\cdot dx, \tag{5}$$

and is integrated over the length of the eddy. The probability of an eddy with a given size occurring is defined by its probability density function

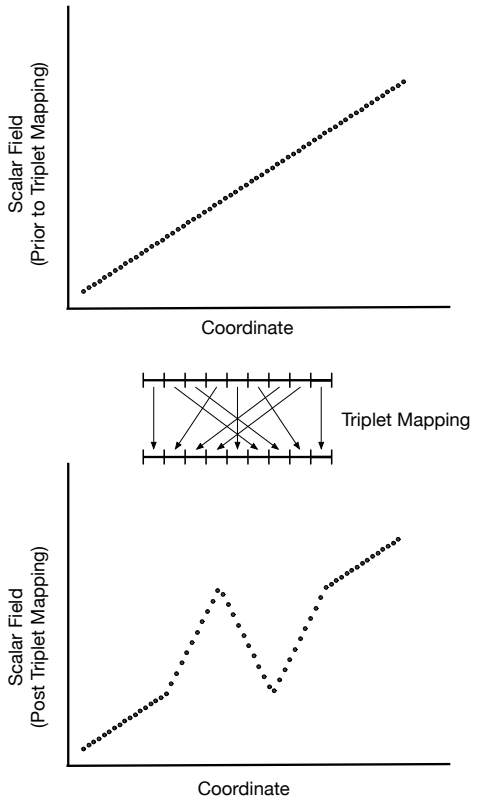

Figure 2: An example of a scalar field undergoing a triplet mapping rearrangement.

$$p = \frac{\lambda(l,\, x_0; t)}{\int\int \lambda \cdot dl\, dx_0}. \tag{6}$$

This is defined as

$$\lambda = \frac{C}{l}\sqrt{\left(\hat{u_i}^2 + \hat{u_j}^2 + \hat{u_k}^2 - Z\left(\frac{u}{l}\right)^2\right)} \tag{7}$$

where C is the eddy rate constant and Z is an eddy suppression mechanism to disallow the smallest eddies. The eddy rate constant, C, is an important parameter, as it drives the number of eddy events.

2.3 Cross Line Flux Resolution

A line oriented in the x-direction will not contain fully resolved fluxes in the y and z-directions. We can break the total flux into its components, as shown in (8). Three sets of governing equations will need to be solved, one associated with each bundle direction. However, only the flux in the direction of the bundle is fully resolved. Taking the flux term from (1) and expanding,

$$-\int_{\mathsf{S}} (\boldsymbol{\Theta}_\psi \cdot \mathbf{n})\, \mathrm{d}\mathsf{S} = -\int_{\mathsf{S}} (\boldsymbol{\Theta}_{\psi,1} \cdot \mathbf{n}_1 + \boldsymbol{\Theta}_{\psi,2} \cdot \mathbf{n}_2 + \boldsymbol{\Theta}_{\psi,3} \cdot \mathbf{n}_3)\, \mathrm{d}\mathsf{S}, \tag{8}$$

we see that solving the governing equations on a specific bundle will require resolution of fluxes perpendicular to the bundle direction. These fluxes can be obtained from nearby orthogonal lines within a coarse control volume. However, the limitation of this approach is that these will be low-wavenumber fluxes. Instead, we can construct high-wavenumber fluxes by decomposing a flux into $\mathbf{n}_\psi = \bar{\mathbf{n}}_\psi + \mathbf{n}'_\psi$, where $\mathbf{n}_\psi$ is the total flux of ψ. $\bar{\mathbf{n}}_{\psi,1}$ is the fully resolved, but spatially filtered, flux obtained from the x_1-bundle line. Nearby orthogonal lines will provide $\mathbf{n}'_\psi$, which is the high-wavenumber flux, with a mean of zero. In this way, we will construct fluxes that are fully resolved across coarse volumes but still capture high-wavenumber fluctuations. This is analogous to a synthetic field approach. For example, the x-direction flux on the x-bundle, $\Theta_{\psi,1}$,

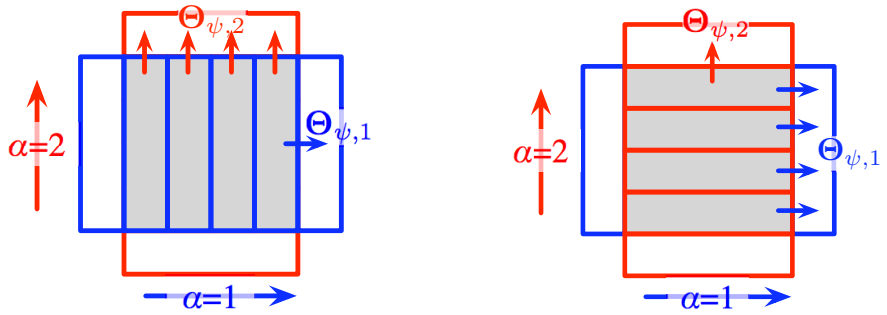

(a) Fluxes associated with x-oriented control volumes

(b) Fluxes associated with y-oriented control volumes

Figure 3: Fully resolved and high wave-number fluxes in the x and y direction

as shown in Figure 3a, is fully resolved but only contains low-wavenumber information. By subtracting the high-wavenumber flux, $\Theta_{\psi,1}$, obtained from the y-bundle shown in Figure 3b, from the fully resolved flux, a synthetic field is constructed.

3 Verification And Results

3.1 Dynamic Eddy Rate Constant

This project has investigated the effects on the eddy rate parameter. This parameter, C, is fundamental to controlling the "eddy events" associated with ODT modeling. For Reynolds numbers above $Re > 9000$, where turbulence is fully developed, an eddy rate constant of $C = 10$ allows stand alone ODT models to accurately capture the effects of turbulence. However, at Reynolds numbers between $2250 > Re > 9000$, in the transitional regime, the eddy rate constant must be increased in order to ensure that enough triplet mapping events are produced. While current literature in this area is lacking, preliminary research suggests an empirical formulation,

$$C = \begin{cases} 10 & Re > 9000 \\ bRe^a & 2250 \leq Re \leq 9000 \end{cases}$$

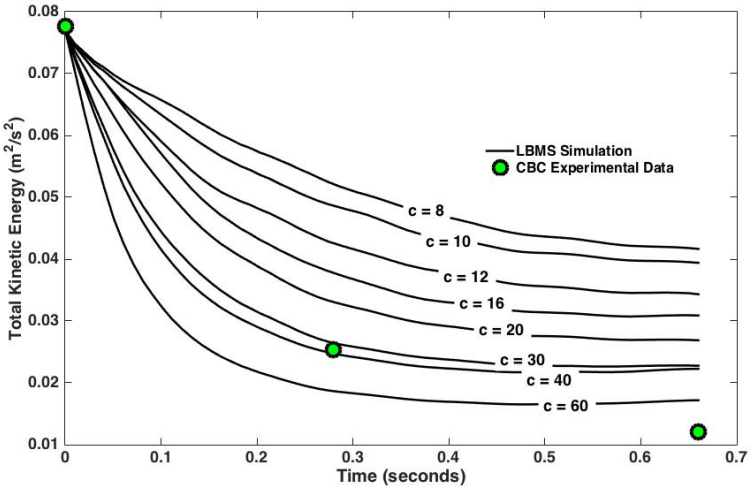

Figure 4: Isotropic Turbulence Decay with [4, 4, 4] coarse points and [512, 512, 512] fine grid points. The Eddy Rate Constant, C, is increased from 8 to 60. Experimental data points at $t = 0$, 0.28 and 0.66 s.

where $a = -1.49$ and $b = e^{15.1}$, represents this transitional regime appropriately [15]. When attempting to reproduce the kinetic energy decay from the Comte-Bellot and Corrsin grid generated isotropic turbulence experimental data, the decreasing Reynolds number has given LBMS issues, as shown in Figure 4. This corroborates other research that suggests that the eddy rate constant must increase as the Reynolds number decreases [16, 17]. As such, a dynamic eddy rate constant will need to be implemented. This area is ripe for investigation, not just for LBMS but for traditional ODT as well. However, as LBMS is a three-dimensional model that consists of many ODT lines, it may be particularly important to have eddy rate constants local to each individual ODT line within a bundle.

3.2 Verification of the Turbulence Modeling

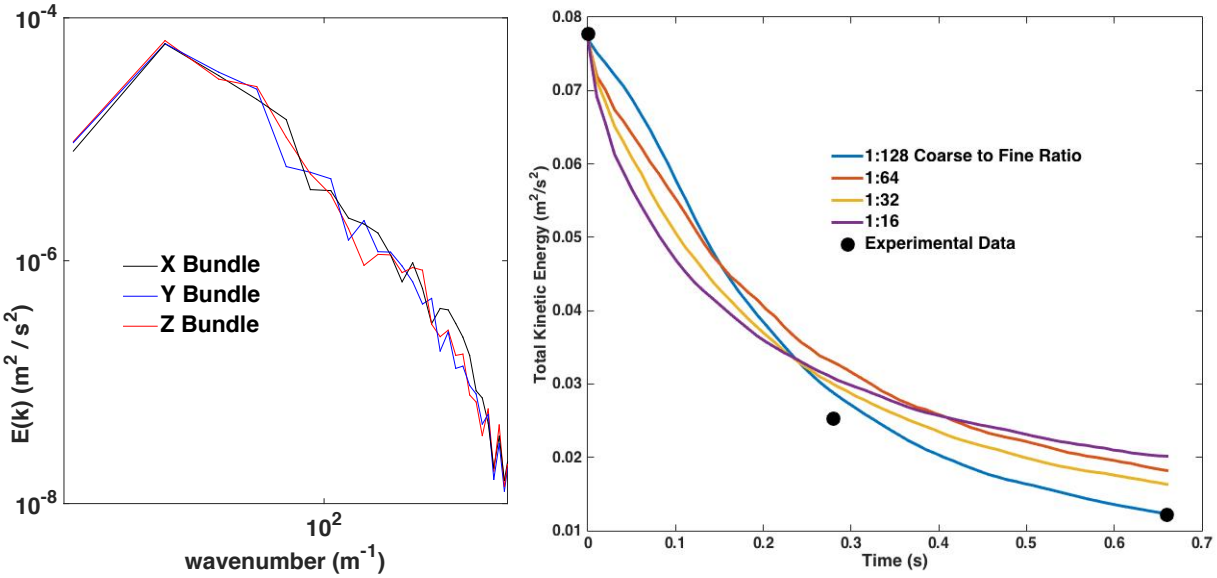

(a) Kinetic energy spectra in wave space for each bundle with a coarse to fine grid spacing of $8/512$.

(b) Kinetic energy decay across a range of coarse to fine scalings.

Figure 5: Verification of LBMS in modeling isotropic turbulence decay.

LBMS can accurately capture the turbulent kinetic energy spectra across a range of scales as well as the appropriate decay of the total kinetic energy for isotropic turbulence. Initial conditions are created using a synthetic turbulence generator, matching the kinetic energy of experimental grid generated turbulence data [18]. The kinetic energy spectra in wave space, as shown in Figure 5a, exhibits the $-5/3$ scaling law across the inertial range scales.
Furthermore, LBMS exhibits kinetic energy decay which qualitatively matches the experimental data across a range of coarse to fine ratios, as seen in Figure 5b. There are non-negligible differences between coarse ratios in the kinetic energy decay. These differences, however, pale in comparison to the variation created by the eddy rate parameter, as shown in Section 3.1.

3.2.1 Triplet Mapping Within LBMS

The implementation of ODT in LBMS is rather straight forward. The triplet mapping is formulated similarly to a traditional three velocity ODT model. However, LBMS can potentially capture the coarse effects of turbulence twice. The coarse fields will simulate the coarse scales of 3D turbulent mixing concurrently with the ODT triplet mapping. To ensure that energy is not pushed from the large scales into the smaller scales at an unphysical rate, eddy events that model information that already exists at the coarse scales will be removed. Eddies larger than $L_{max} = 3.5 \cdot \Delta$ coarse cell volumes are excluded. This was chosen due to the nature of information exchange created by the triplet map, shown in Section 2.2. As quantities are

rearranged, the furthest they travel is $1/3$ of the length of the eddy. $L_{max} = 3 \cdot \Delta$ coarse volumes, as shown in Figure 6, was simply not adequate, however. Energy gathers in the resolution gap between the coarse

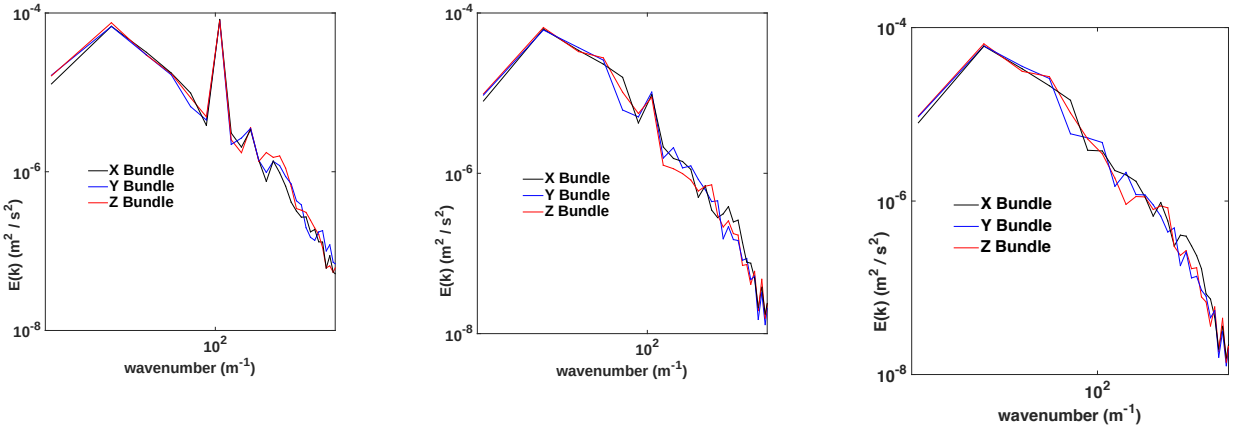

(a) Removal of eddies larger than Δ (b) Removal of eddies larger than $3 \cdot \Delta$ (c) Removal of eddies larger than $3.5 \cdot \Delta$

Figure 6: Kinetic energy spectra of simulations comparing the maximum eddy sizes allowed. This case was an Isotropic Turbulence initial condition (See Section 3.2) run with a coarse grid spacing of $\Delta = 0.052\, meters$.

length scales and the modeled length scales. This is because one coarse volume can only contain its own information. Therefore, a slightly larger value, $L_{max} = 3.5 \cdot \Delta$, was chosen. Previous research on ODT-LES chose the max eddy length of $L_{max} = 4 \cdot \Delta$ [17].
Furthermore, triplet mapping can increase or decrease conserved quantities within a coarse volume, $\Delta^{(x)}\Delta^{(y)}\Delta^{(z)}$, if the triplet mapping exchanges information across one or more volumes. While ODT ensures that these quantities are conserved along an individual line [2], conservation is not guaranteed on intersecting lines. To maintain consistency, the change in the integral of the conserved quantities from before and after an eddy event is enforced on intersecting lines, as shown by Equation 9,

$$\underbrace{\int \rho\psi \, dV_\Delta}_{Perpendicular\ Line} = \underbrace{\int \rho\psi \, dV_\Delta}_{Post\ Eddy} - \underbrace{\int \rho\psi \, dV_\Delta}_{Prior\ to\ Eddy} \tag{9}$$

where V represents the coarse volume that these lines intersect.
Finally, investigations have shown that such an application of conservation principles can create sharp gradients at the boundary of coarse volumes on perpendicular lines in the perpendicular direction to the triplet mapping after conservation is enforced. As such, a simple moving triangular filter with a width of Δ is applied and scaled such that Equation 9 is not invalidated.

3.3 Flux Reconstruction

As discussed in Section 2.3, consistency of orthogonal fluxes will be maintained by enforcing Equation 8 through communication of the fully resolved fluxes from orthogonal ODT lines. This can be accomplished in a variety of ways. The coarse flux could be superimposed upon the fine fluxes. Equation 10,

$$\Theta^{(y)}_{x,\, reconstructed} = \frac{\Theta^{(x)}_x}{\delta/\Delta}, \tag{10}$$

shows how an x-flux on a y-bundle can be reconstructed. However, this treatment will coarsen the resulting fluxes, which will cause a loss of high wave-number information. One possible solution is to satisfy the

equality given in Equation 8 while still including the under-resolved but high wave-number information. Equation 11,

$$\Theta^{(y)}_{x,\,reconstructed} = \frac{\Theta^{(x)}_{x}}{\delta/\Delta} + \Theta^{(y)}_{x} - \sum_{i=1}^{\delta/\Delta} \Theta^{(y)}_{x,\,i}, \tag{11}$$

shows a possible reconstruction that utilizes the under-resolved fluxes to recreate a high wave-number flux while still maintaining consistency.

3.4 Parallelization and Scaling Results

LBMS ultimately has three meshes, composed of a series of parallel lines, that cover the whole domain, one associated with each bundle direction. These meshes communicate flux and triplet mapping information with each other. Therefore, domain decomposition involves partitioning each of the three meshes onto a given number of processors. As the problem is divided up into directional bundles by dimension there will of necessity be processor counts which perform better than others. This creates noise in the scalability as load imbalances at various processor counts affect the scaling results. In addition to processor count and problem size, there is also the issue of the fine to coarse ratio, Δ/δ , to consider in scaling. Volumetric communication occurs on the Δ-scale, so it is important, from a scalability perspective, to maintain relatively large Δ/δ.

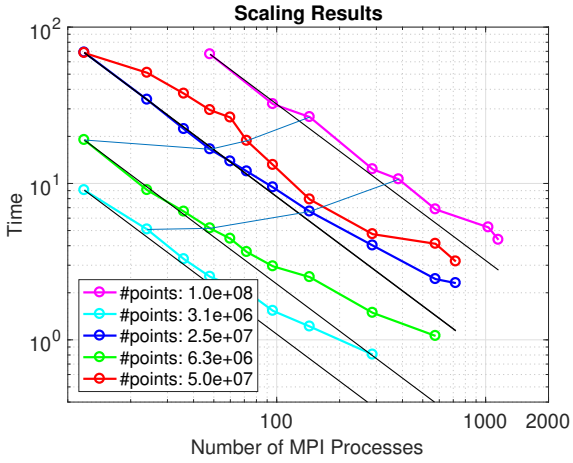

Figure 7: Scaling results.

Figure 7 shows results of scaling on a variety of coarse to fine ratios and domain sizes. It is interesting to note that the scaling profile behaves in a similar fashion across differing ratios. Weak scaling lines on the plot include points on all intersecting lines, showing differences in different coarse to fine ratios. These ratios affect performance, as seen on the graph though they still perform similarly to each other.

3.5 Timings

For Lattice-Based Multiscale Simulation (LBMS) to compete with Direct Numerical Simulation (DNS) and Large Eddy Simulation (LES), reasonable speed up must be obtained as the number of grid points is decreased through coarsening. The fine grid spacing, δ_{LBMS}, however, is constrained by the turbulent length scales in order for the One-Dimensional Turbulence (ODT) model to appropriately resolve eddies down to the smallest length scales. However, the perpendicular flux reconstruction treatment, which utilizes fully resolved coarse fluxes from other bundles as well as high wave number fluxes from the native bundle, will not necessarily decrease in cost with a decrease in the number of course grid cells.

We investigated computational speed ups by maintaining 256 fine grid points while varying the fine to coarse ratio, $\delta_{LBMS}/\Delta_{LBMS}$, between $1/2$, $1/4$, $1/8$, $1/16$, $1/32$, and $1/64$. This case was a cold flow, compressible simulation with periodic

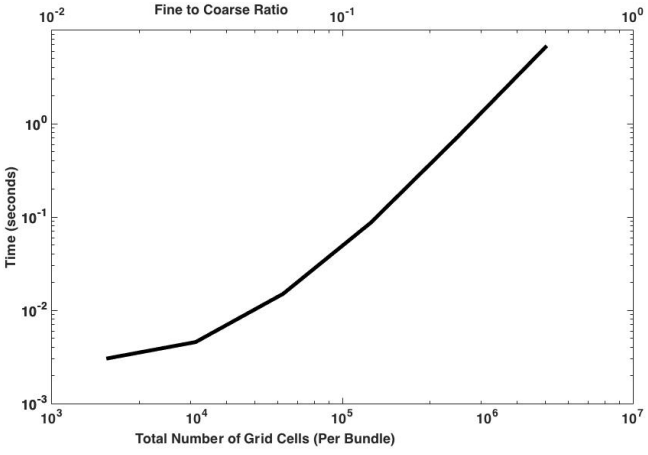

Figure 8: Average time to execute a single time step while varying the coarse grid spacing (i.e. the number of ODT lines on each bundle).

boundary conditions. The results were obtained by running the case on three processors. This ensures that communication between processors must occur, as each bundle, the $x - bundle$, $y - bundle$ and $z - bundle$, is decomposed onto its own core. Figure 8 shows that, as LBMS coarsens, flux reconstruction does indeed begin to dominate the computational costs. However, even when coarsening from $1/32$ to $1/64$, there is still a 49% speed up. The bottom axis shows the total number of points on each bundle while the top axis shows the ratio. For example the fastest case has 256 by 4 by 4 control volumes for a total of 4096 cells on its $x - bundle$. For this same case, the ratio is $1/64$. This speedup shows that, while an asymptotic limit may exist, dramatic coarsening still provides a significant reduction in computational costs. As such, LBMS has the potential to be a viable method for reducing the high computational costs often associated with turbulent flow simulations.

3.6 Filtering

Eddy events in ODT are ultimately instantaneous. If a physical eddy has an eddy turnover time of 1 s, a triplet mapping of the same length should be applied once per second if the ODT parameters are tuned correctly. However, the acoustics of that eddy will be released between the simulation time step in which it occurs. In LBMS, this may cause issues if two ODT lines produce eddies concurrently. There is potential for constructive interference with two such eddy events "popping" near each other in space and time. As such, a high wave-number filter was investigated in order to reduce this effect. This order n filter is defined as

$$\hat{U} = (1 - \alpha_D D)\, U \tag{12}$$

where U is the unfiltered quantity, D is a spatial discretization matrix and α_D is defined by

$$\alpha_D = (-1)^n\, 2^{-2n}. \tag{13}$$

However, such a filter was found to be both unnecessary and had the potential to increase instability. By applying any filtering, aliasing of high wave-number information could occur. Additionally, eddy events often are rare enough and far enough apart in time and space to have acoustic noise dissipate prior to the point at which constructive interference would occur.

4 Tools for Analysis of Chemical Dynamics

4.1 Web-Application for Zero-Dimensional Reactor Simulation

In connection with a senior design project for computer science students, we have developed a robust, efficient, web-based tool for parametric simulation of zero dimensional reactors with finite residence time. This leverages recent advances in robust time integration for combustion chemistry [19, 20] to provide a convenient way of analyzing chemical mechanisms and obtaining physical insight into the behavior of large mechanisms such as those for biofuels.

This web interface allows the user to specify different chemical mechanisms, residence times, as well as initial temperature, pressure and species mole fractions as parametric inputs and can provide either transient or steady-state solutions. This work was presented at the SIAM International Numerical Combustion Meeting in April 2017 in Orlando, Florida [21].

4.2 Stiffness Reduction via Principal Component Analysis

Finally, we have provided formal analysis of principal component analysis (PCA) based modeling frameworks recently proposed [22, 23]. The motivation for this work came from the empirical observations from previous work that suggest when PCA is used to reduce the dimensionality of a system, it also reduces the stiffness.

We have studied stiffness of the original system as well as a reduced PC-space systems by comparing eigenvalues of the Jacobian matrices of the conserved chemical source terms and of the principal components once the PC space has been truncated. Two methods are evaluated for obtaining the Jacobian in PC space: performing a similarity transformation on the Jacobian in state space using the PCA transformation matrix and using a finite-differenced Jacobian from the regression of the source terms in PC space on the PCs.

Autoignition training data for adiabatic, constant volume batch reactors was first generated. Variables that did not deviated from zero were removed, and the remaining variables were centered and scaled before applying PCA. Timescales (inverse eigenvalues) were then compared for the two methods of obtaining the Jacobian in PC space with the Jacobian in state space.

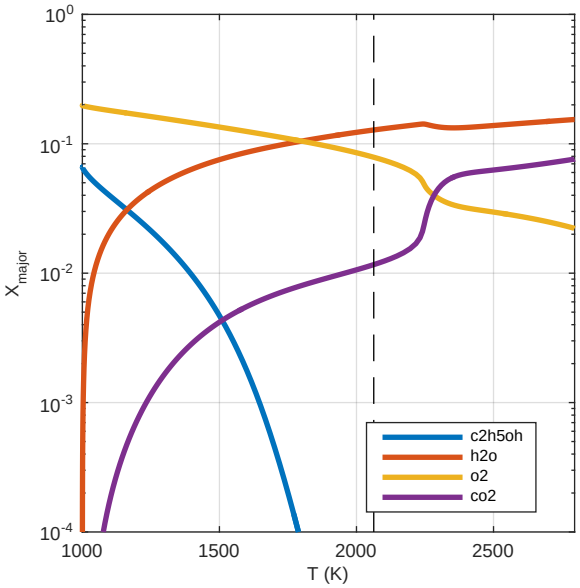

(a) Major species mole fraction profiles versus temperature.

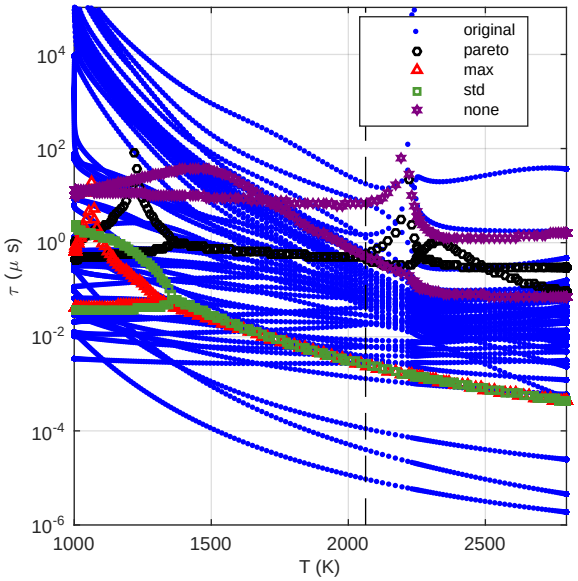

(b) Eigenvalues, τ over temperature with two retained PCs.

Figure 9: Ethanol autoignition event in air at 1000 K, one atm. The dashed black line shows the temperature at the ignition delay.

Results for a 57-species ethanol m[24, 21, 25]echanism are shown in Figure 9 for the similarity transform method with different PCA scalings, which shows that PCA eliminates the fastest timescales, thereby reducing stiffness in the resulting system. We also found that the timescales in PC space, regardless of the method used to calculate them, show sharp peaks at various times during the autoignition events. This suggests that, when using an implicit time integrator, it may be difficult to reach a physically realizable solution in PC space for autoignition. Future work will explore the performance of these cases in solving the governing equations in PC space compared to those in state space. Including more training data as well as possibly training with steady flamelets or one-dimensional premixed systems could result in better manifolds in PC space, reducing the nonlinearities in the timescales. This work was presented at the US National Combustion meeting in April, 2017 [25].

5 Conclusion and Accomplishments

This project has led to several publications and presentations [26, 27, 24, 21, 25], and has explored new techniques for high-fidelity turbulent combustion simulation.

By utilizing a very powerful model in ODT, LBMS has the potential to drastically reduce the three-dimensional costs of DNS while still capturing the turbulent diffusive interactions. ODT has proven itself against a variety of difficult problems, leading to many possible uses for LBMS. This model improves on ODT by overcoming its inability to capture large scale three dimensional effects while still maintaining its most important feature, dimensional reduction. LBMS resolves turbulent interactions across all range of scales that traditional LES simulations cannot.

This project has established the framework and investigated many issues that arise when coupling many ODT lines that span multiple dimensions. It has shown that through coupling perpendicular ODT lines and

coarsening the spacing between said lines, LBMS can capture kinetic energy spectra and decay associated with turbulent statistics. This project was not able to fully investigate turbulent combustion due to unexpected issues arising when coupling each bundle to one another but it has investigated and overcome fundamental issues, which will lead the way to LBMS bridging the gap between DNS and LES in terms of computational tenability and fidelity.

Finally, this project has also made contributions in systematic model reduction for combustion through principal component analysis [21, 25].

References

[1] Naveen Punati, James C Sutherland, Alan R Kerstein, Evatt R Hawkes, and Jacqueline H Chen. An evaluation of the one-dimensional turbulence model: Comparison with direct numerical simulations of CO/H2 jets with extinction and reignition. *Proceedings of the Combustion Institute*, 33(1):1515–1522, 2011.

[2] Alan R. Kerstein. One-dimensional turbulence: model formulation and application to homogeneous turbulence, shear flows, and buoyant stratified flows. *Journal of Fluid Mechanics*, 392:277–334, aug 1999.

[3] Wm T Ashurst, Alan R Kerstein, Wm T Ashurst, and Alan R Kerstein. One-dimensional turbulence : Variable-density formulation and application to mixing layers. *Physics of Fluids*, 17, 2005.

[4] Naveen Punati, James C Sutherland, Alan R Kerstein, Evatt R Hawkes, and Jacqueline H Chen. An Evaluation of the One-Dimensional Turbulence Model: Comparison with Direct Numerical Simulations of CO/H2 Jets with Extinction and Reignition. *Proceedings of the Combustion Institute*, 33:1515–1522, 2011.

[5] T. Echekki, A. R. Kerstein, T. D. Dreeben, and J. Y. Chen. One-Dimensional Turbulence Simulation of Turbulent Jet Diffusion Flames: Model Formulation and Illustrative Applications. *Combust. Flame*, 125:1083–1105, 2001.

[6] S. B. Pope. *Turbulent Flows*. Cambridge University Press, New York, 2000.

[7] Ugo Piomelli and Elias Balaras. Wall-layer models for Large Eddy Simulations. *Annual Review of Fluid Mechanics (2002)*, 34(1):349–374, 2002.

[8] Alan R. Kerstein, W. T. Ashurst, Scott Wunsch, and Vebjorn Nilsen. One-dimensional turbulence: vector formulation and application to free shear flows. *Journal of Fluid Mechanics*, 447:85–109, oct 2001.

[9] Alan R. Kerstein. Linear-eddy modelling of turbulent transport. Part 6. Microstructure of diffusive scalar mixing fields. *Journal of Fluid Mechanics*, 231:361, 1991.

[10] Niveditha Krishnamoorthy. *Reaction Models and Reaction State Parameterization for Turbulent Non-Premixed Combustion*. Ph.d. thesis, University of Utah, 2008.

[11] B Ranganath and T Echekki. One-Dimensional Turbulence-based closure for turbulent non-premixed flames Bhargav Ranganath and Tarek Echekki *. *Progress in computational fluid dynamics.*, 6(7):409–418, 2006.

[12] David O Lignell, Garrison C Fredline, and Adam D Lewis. Comparison of one-dimensional turbulence and direct numerical simulations of soot formation and transport in a nonpremixed ethylene jet flame. *Proceedings of the Combustion Institute*, 35(2):1199–1206, 2015.

[13] Babak Goshayeshi and James C Sutherland. Prediction of oxy-coal flame stand-off using high-fidelity thermochemical models and the one-dimensional turbulence model. *Proceedings of the Combustion Institute*, 35(3):2829–2837, 2015.

[14] Alex W Abboud, Ben B Schroeder, Tony Saad, Sean T Smith, Derek D Harris, and David O Lignell. A Numerical Comparison of Precipitating Turbulent Flows Between Large-Eddy Simulation and One-Dimensional Turbulence. *AIChE*, 00(00), 2015.

[15] Naveen Punati. *An Eulerian One-Dimensional Turbulence Model : Application to Turbulent and Multiphase Reacting Flows*. PhD thesis, University of Utah, 2012.

[16] Esteban D. Gonzalez-Juez, Rodney C. Schmidt, and Alan R. Kerstein. ODTLES simulations of wall-bounded flows. *Physics of Fluids*, 23(12):125102, 2011.

[17] Rodney C. Schmidt, Alan R. Kerstein, and Randall McDermott. ODTLES: A multi-scale model for 3D turbulent flow based on one-dimensional turbulence modeling. *Computer Methods in Applied Mechanics and Engineering*, 199(13-16):865–880, feb 2010.

[18] Stanley Corrsin and Geneviève Comte-Bellot. Simple Eulerian time correlation of full- and narrow-band velocity signals in grid-generated, isotropic turbulence. *Journal of Fluid Mechanics*, 48(2):273–337, 1971.

[19] M A Hansen and J C Sutherland. Pseudotransient Continuation for Combustion Simulation with Detailed Reaction Mechanisms. *SIAM Journal on Scientific Computing*, 38(2):B272–B296, jan 2016.

[20] Michael Alan Hansen and James Clayton Sutherland. Dual timestepping methods for detailed combustion chemistry. *Combustion Theory and Modelling*, pages 1–17, oct 2016.

[21] E. Armstrong, M. A. Hansen, and J. C. Sutherland. A Web-Based Tool for Simulation and Numerical Analysis of Zero-Dimensional Combustion Problems. In *16$^{\text{th}}$ Intl. Conference on Numerical Combustion*, Orlando, FL, April 2017.

[22] J. Sutherland and A. Parente. Combustion modeling using principal component analysis. *Proc. Combust. Inst.*, 32(1):1563–1570, 2009.

[23] Amir Biglari and James C Sutherland. An a-posteriori evaluation of principal component analysis-based models for turbulent combustion simulations. *Combustion and Flame*, 162(10):4025–4035, oct 2015.

[24] Tony Saad, Derek Cline, James C. Sutherland, and R. Stoll. Scalable Tools for Generating Synthetic Isotropic Turbulence with Arbitrary Spectra. *AIAA journal*, 55(1):327–331, 2017.

[25] E Armstrong, M A Hansen, and J C Sutherland. Assessment of Stiffness Reduction in Chemical Reacting Systems Using Principal Component Analysis. In *10$^{\text{th}}$ US National Combustion Meeting*, College Park, MD, April 2017.

[26] Derek Cline, James C. Sutherland, and Tony Saad. Lattice based multiscale simulation. In *SIAM Computational Science and Engineering Conference*, page poster, http://www.siam.org/meetings/cse15/, March 2015.

[27] John Hutchins, Derek Cline, and James C. Sutherland. A task-parallel approach for solving PDEs on a lattice. In *SIAM Computational Science and Engineering Conference*, page poster, http://www.siam.org/meetings/cse15/, March 2015.